ISSN: 0974-2115
www.jchps.com Journal of Chemical and Pharmaceutical Sciences

A Complete Synergy on the Experimental and Theoretical Investigation of 4-Nitroaniline for Nonlinear Optical Applications

K. Sangeetha[1], L. Guru Prasad[2], R. Mathammal[1*]
[1]Department of Physics, Sri Sarada College for Women, Salem-16
[2]Department of Science & Humanities, M. Kumarasamy College of Engineering, Karur.
***Corresponding author: E-Mail:mathammals_shanmugam@yahoo.com, Tel. +91 9944 612730**

ABSTRACT

Single crystals of 4-nitroaniline ($C_6H_6N_2O_2$) have been developed by using slow evaporation solution technique. The lattice parameters of the 4NA crystal are confirmed by analysing the single crystal XRD data. Quantum chemical calculations have been performed in B3LYP/6-31+ G (d, p) method. Presence of functional groups and their vibrational characteristics were studied from the vibrational spectrum. Optical absorption behaviour of the 4NA crystal was examined and value of the energy gap is also estimated. Computational studies show that the 4NA molecule possesses non-zero first order hyper polarizability. Kurtz and Perry (1968), powder technique was used to confirm the SHG efficiency of crystal. Molecular orbital analysis reveals the charge transfer nature of the 4NA compound.

KEY WORDS: 4-nitroaniline, Vibrational analysis, NMR, NBO analysis, NLO, HOMO- LUMO energy.

1. INTRODUCTION

Organic materials exhibit nonlinear optical (NLO) properties are very useful in the field of photonics, with a view of expanding its application (Prasad and Williams, 1991). Organic materials consist of many advantages over the inorganic materials, it has a larger response time and it shows high hyper polarizability values. Among the available organic materials nitro group compounds have been attracted because of its high nonlinear coefficients (Williams and Angrew, 1984).

Aniline and much of its derivatives are widely utilizing for the preparation of pharmaceutical compounds Palafox, (2002). In aniline, the planarity of the molecule is affected by the amino group and if an additional substituent group is included in aniline, further changes occurs in the charge distribution which affects the structural and vibrational parameters. This charge transfer characteristic is very much useful to get the high nonlinear coefficients. Among the aniline groups, nitroaniline is used in the synthesis of pharmaceuticals, rubber, dyes and coccidiosis. Nitroanilines (NA) are very good examples of push–pull molecules due to the intra-molecular charge transfer from the electron-donor (NH_2) to the electron-acceptor (NO_2) group. Because of the push-pull character these compounds may show frequency conversion characteristic. In this view we decided to grow 4-nitroaniline (4NA) crystal. The intend of the present investigation is to give a complete description of the 4NA molecule.

2. EXPERIMENTAL DETAILS

Crystal growth: The compound 4NA was purchased from Sigma-Aldrich Chemical Company (U.S.A) with a purity of 99% and is used to grow the crystals. Crystals of 4NA have been grown by slow evaporation solution technique. Saturated solution of 4NA was prepared in ethanol using magnetic stirrer and the solution is filtered to eradicate the impurities present. The solution which was filtered is covered with perforated foil and was kept undisturbed. Evaporation of solvent yields the transparent yellow crystals of 4NA in 7 days and as grown crystal is depicted in the Fig.1.

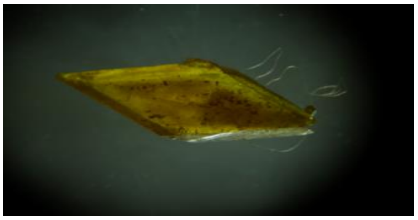

Figure.1. The grown single crystal of 4NA

Computational Details: All the computational calculations has been carried at Density functional theory (DFT) level B3LYP/6-31+ G (d, p) (Hohenberg, 1964; Becke, 1993; Lee, 1998), using Gaussian 09 Frisch, (2009) program package, invoking gradient geometry optimization. Vibrational frequency assignments have been determined by using the Gaussview Frisch, (2000) software. According to the work of Rauhut and Pulay (1995), a scale factor of 0.96 is applied for the vibrational studies in the 4NA compound. The optimized structure has been taken for NBO analysis, NMR, hyperpolarizability and MEP studies.

3. RESULTS AND DISCUSSION

Single crystal XRD: Single crystal XRD data of the 4NA crystal has been recorded using Enraf–Nonius CAD4 diffractometer with Mo Kα with the λ = 0.71073 Å. The structure is solved by direct methods using SHELXS97.

Geometry of the 4NA molecule is determined using the Jain, (1980) and Rastogi, (2002) software's. Single crystal XRD data reveals that 4NA crystal crystallize in monoclinic system. The crystallographic data and structure refinement information are tabulated in Table.1. Fig.2, shows the ORTEP view of the molecule.

Table.1. Crystal data and structure refinement for the 4NA crystal

Empirical formula	$C_6H_6N_2O_2$
Formula weight	138.13
Temperature	293(2) K
Wavelength	0.71073 A
Crystal system, space group	Monoclinic, P21/n
Unit cell dimensions	a = 8.5789(5) Å alpha = 90°. b = 6.0258(4) Å beta = 91.549(7)° c = 12.3048(8) Å gamma = 90°
Volume	635.86(7) A^3
Z, Calculated density	4, 1.443 Mg/m^3

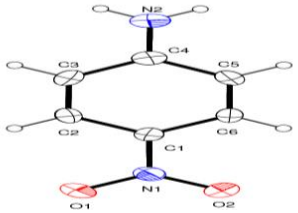

Figure.2. The ORTEP structure for 4NA

Vibrational analysis: Vibrational spectral assignments were performed based on the theoretical calculation and are tabulated in Table 2. The 4NA molecule consists of 16 atoms and so it has 42 normal vibrational modes. The point group for 4NA is C_1 point group with 42 degrees of freedom. All the vibrations are active in IR and Raman. Figs.3 & 4, shows the experimental and computed FT-IR spectra and Raman spectra. Table.2, represents the complete vibrational frequencies and assignments as well as IR and Raman activities.

Table 2. Detailed assignment of fundamental vibrations of 4-NA by normal mode analysis based on SQM force field calculations

Symmetry Species	**Observed frequencies (cm^{-1})**		**Calculated frequencies (cm^{-1}) with B3LYP/ 6-31+ G (d, p) force field**				**%PED**
	Infrared	Raman	Unscaled (cm^{-1})	Scaled (cm^{-1})	IR	Raman	
A	3540	3545	3713	3550	23	78.632	νNH(97)
A	3434	3436	3598	3440	62.51	277.74	νNH(98)
A	3100	3098	3244	3101	2.15	106.70	νCH(97)
A	-	3095	3244	3101	0.2380	27.19	νCH(98)
A	3045	3038	3188	3047	12.48	116.59	νCH(95)
A	3041	-	3187	3046	11.98	71.47	νCH(96)
A	1613	1612	1693	1618	298.44	89.63	βNH_2(64), νCC(12), νCN(10)
A	1580	1583	1657	1584	105.63	2.686	νNO(62), νCC(12), βCNO(10)
A	-	1577	1655	1582	26.51	40.49	νCC(60), βNH_2(12), βCH(10)
A	1528	1530	1603	1532	106.64	5.78	νCC(60), νNO_2(12),βCNH(10)
A	-	1473	1546	1478	39.97	21.25	νCC(62), νCN(22)
A	1420	-	1488	1422	0.297	1.097	νCC(32), βCH(22), βCNH(10)
A	1330	1328	1392	1330	0.157	0.5851	νCC(66), βCNH(10)
A	1320	1318	1390	1329	496	446.6	νNO (64),νCN(12), βONO (10)
A	1265	1261	1344	1285	175.76	35.43	νCN(66), βRing(10), νCC(10),
A	1270	1273	1334	1275	0.1885	0.3470	νCN(72), βCNH(12)
A	1156	1155	1210	1157	17.02	4.539	βCH(62), νCN(10),
A	1098	1095	1150	1099	12.07	1.771	βCH(72), βCNH(10),
A	1085	-	1138	1088	97.85	44.46	βCH(72), βRing(12), νCN(10),
A	1023	-	1071	1024	2.168	1.138	βCH(70),βNH_2(12), βCNH(10)
A	975	976	1022	977	0.302	2.471	βRing(74), βCH(12)
A	935	938	981	938	1.424	2.599	δCH(70), τRing(10)

A	926	927	972	929	0.003	0.173	δCH(90)
A	837	835	875	837	21.48	41.44	βONO(76),νCN(12),βRing(10)
A	803	807	848	810	39.91	0.3004	δCH(82)
A	784	785	824	787	4.97	1.0594	βRing(70),βONO(12),νCN(10)
A	783	-	822	785	0.113	7.158	δCH(90)
A	723	724	757	724	26.88	1.707	δCN(60), τRing(10),τONO(10)
A	660	663	700	669	6.35	0.6020	δCN(64), τRing(10),τONO(10)
A	615	618	648	619	0.745	6.529	βRing(70)
A	610	-	643	614	8.582	1.4053	τRing(70), νCN(12)
A	-	515	540	516	2.208	2.727	βCNO(62), βRing(10)
A	483	-	508	485	9.19	0.824	τRing(58), δCH(12), δCN(10)
A	406	405	426	407	418.9	21.67	δNH_2(64)
A	404	-	425	406	0.325	0.033	τRing(52)
A	375	376	396	378	0.3840	0.3455	βCNH(56)
A	358	357	375	358	13.0026	0.8281	τNH_2(60)
A	348	-	365	349	3.9537	1.1065	βRing(56)
A	277	-	292	279	9.7416	0.7248	τRing(62), τNH_2(12)
A	-	-	227	217	0.4050	0.8974	βONO(50),τNH_2(14),τRing(12)
A	-	-	113	108	0.4248	1.0936	τNH_2(44), τRing(12)
A	-	70	74	70	0.1005	0.3947	τNO_2(42),τNH_2(10),τRing(10)

ν - stretching vibrations, β - bending vibrations, τ - torsional vibrations, δ- out of plane

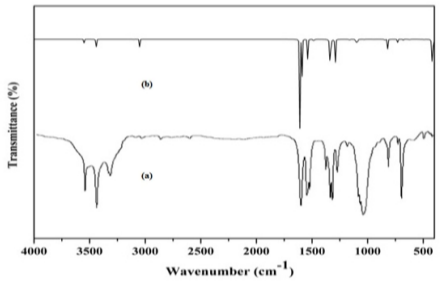

Figure.3. (a) Observed and (b) calculated FT-IR spectra of 4-NA

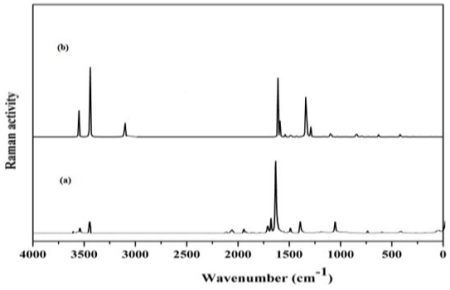

Figure.4. (a) Observed and (b) calculated FT-Raman spectra of 4-NA

C-H Vibrations: The 4NA molecule gives rise to C-H stretching, in-plane bending and out-plane bending vibrations. In the FT-IR spectrum, the peaks traced at 3100, 3045, 3041 cm^{-1} and in the FT-Raman spectrum peaks at 3098, 3095, 3038, cm^{-1} are allotted to C-H stretching vibrations. The aromatic C-H in- plane bending of benzene appeared in the region 1300-1000 cm^{-1}. These bands are sharp but are in weak to a medium intensity. The C-H out- plane bending vibrations and generally it traces peak in the region 900–667 cm^{-1}. The peaks traced at 1156, 1098, 1085, 1023 cm^{-1} in FTIR and 1155, 1095 cm^{-1} in Raman are arises due to C-H in-plane bending vibrations. The peaks simulated at 935, 926, 803, 783 cm^{-1} in FTIR and 938, 927, 807 cm^{-1} in FT-Raman spectrum confirms the C-H out-of-plane bending vibrations.

C-C vibrations: The C-C stretching modes generally trace its peak in the range of 1650 to 1200 cm^{-1}. In the 4NA molecule, the wavenumber established in the FTIR spectrum at 1528, 1420, 1330 cm^{-1} and in FT Raman spectrum at 1577, 1530, 1473 and 1328 cm^{-1} are allotted to C-C stretching vibrations. The CCC in-plane bending vibrations are simulated at 975, 784, 615 cm^{-1} in the FTIR spectrum and in the Raman spectrum at 976, 785, 618 cm^{-1}. The CCC out-of-plane bending vibrations are found at low wavenumbers computed at 610, 483, 404 cm^{-1} for FTIR spectrum and the same was absent in Raman spectrum.

C-N vibrations: Recognition of C-N vibrations is quite a very difficult task in the FTIR spectrum, since mixing of several bands are possible in this region. On the other hand with the aid of computational studies, the C-N stretching vibrations have been observed. In 4NA, the bands are identified at 1265 cm^{-1}, 1270 cm^{-1} in the FTIR and at 1261 cm^{-1}, 1273 cm^{-1} in FT-Raman spectrum.

Nitro vibrations: In 4NA, the bands appeared at 1580 cm^{-1} in the FTIR and 1583 cm^{-1} in the FT-Raman spectrum are allotted for asymmetric stretching vibrations of nitro-group. Band observed at 1580 cm^{-1} and 1583 cm^{-1} are assigned to asymmetric stretching vibration which occurs due to the intermolecular hydrogen bonding and inductive effect. The title molecule traces peak at 1320 cm^{-1} in the FTIR and 1318 cm^{-1} in the Raman spectrum and are attributed to symmetric stretching vibration. The deformation vibration bands appeared in the region around the characteristic position 837 cm^{-1} in FTIR and 835 cm^{-1} in Raman spectrum for 4NA.

NH_2 Vibration: Generally, in all the primary aromatic amines, the N-H stretching frequencies occur in the region 3300-3500 cm^{-1}. The 4NA compound consists of one NH_2 group and hence one symmetric and one asymmetric N-H stretching vibrations appeared in the vibrational spectrum. In the title molecule, the band simulated at 3540 cm^{-1} and 3545 cm^{-1} is allotted to asymmetric stretching vibration. In symmetric stretching mode the band established at 3434 cm^{-1} in the FT-IR and at 3436 cm^{-1} in Raman spectrum.

Optical studies: The optical absorbance spectrum is being recorded in the wavelength range of 200–1200 nm using Perkin Elmer Lamda 935 UV–Vis–NIR spectrophotometer at room temperature. Fig.5a, shows the recorded optical absorption spectrum of 4NA crystal in which characteristic absorption band occurs below 400 nm. The thickness of the sample used for measurement was 2 mm. From Fig.5b, it is clearly visible that the 4NA crystal has transparency wider and the lower cutoff wavelength is found at 398nm. Higher transparency and low cutoff in wavelength confirms that 4NA material is very much useful for optical applications. Energy gap of 4NA is determined by using the formula Dillip (2011).

$$E = \frac{1.243X10^3}{\lambda_{max}}\ eV$$

Where, λ is the lower cutoff wavelength and the value of energy gap is calculated as 3.12 eV. Simulated UV-VIS spectrum for 4NA was obtained by using TD-DFT method and the maximum absorption occurs at 240 nm. This peak arises due to the transition of electrons from π-π*. Stimulated UV-Vis-NIR spectrum is visualized in Fig. 5c.

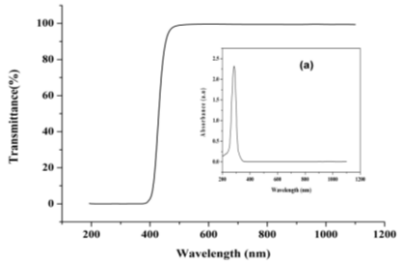

Figure.5. Optical (a) absorbance and (b) transmittance of 4NA single crystal

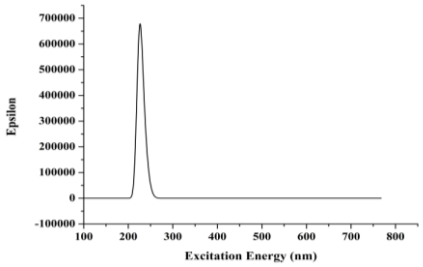

Figure.5(c). Theoretically calculated UV-Vis Spectrum of 4NA

NMR spectral analysis: The ^{13}C and ^{1}H theoretical and experimental chemical shifts of 4NA are tabulated in Table.3 and the NMR spectra of 4-NA are shown in Figs. 6 & 7. Theoretical calculations on chemical shift for optimized 4NA structure were carried out by using GIAO method and compared with experimental data. In 4NA compound, the aromatic protons chemical shift, H8, H7, H10 and H9 are well agreed with the theoretical range of chemical shift. For the title compound, the nitrogen atom is in the para position. This nitrogen atom has electronegative property and the oxygen atom in nitro group of 4NA is electron withdrawing group, hence deshielding occurs and the value of C5 and C2 is high. The other carbon atoms of the benzene structure give the signal at 113.06, 113.05, 97.90 and 97.86 ppm. The aromatic protons have the chemical shift δ (ppm) in the range 6–8.5. The signals at **δ**=8.36ppm and δ=8.35 ppm are due to aromatic protons. Here there is more deshielding and hence the chemical shift increases. The signals at 8.36, 8.35, 6.48 and 6.47 ppm are due to the hydrogen atom in the aromatic ring. Here there is more deshielding arises due to electronegative oxygen atom and it causes increase in the chemical shift. The signal at 3.43 ppm and 3.42 ppm is due to proton of the amine group. As the hydrogen atom is surrounded by electronegative oxygen atoms, there may be more shielding in that region and cause the chemical shift falls at up field with low ppm value. Since, greater is the degree of hydrogen bonding of a proton then greater is the downfield shift.

Table.3. Experimental and calculated ^{13}C NMR and ^{1}H NMR Chemical shifts (ppm) of 4-NA

Atoms	Experimental	B3LYP/6-31+G (d, p)
C_5	155.61	134.96
C_2	135.67	126.48
C_3	126.34	113.06
C_1	112.38	113.05
C_6	-	97.90
C_4	-	97.86
H_8	8.075	8.36
H_7	8.056	8.35
H_{10}	7.259	6.48
H_9	6.632	6.47
H_{15}	6.612	3.43
H_{16}	4.395	3.42

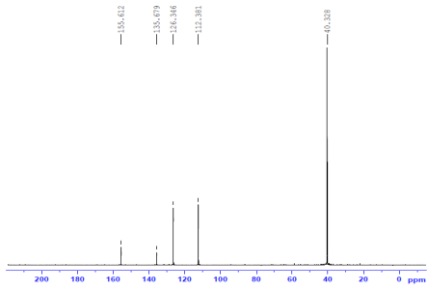

Figure.6. (a) Experimental ^{13}C NMR Spectrum

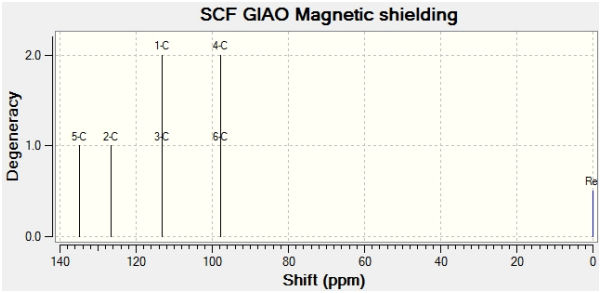

Figure.6. (b) Theoretical ^{13}C NMR Spectrum

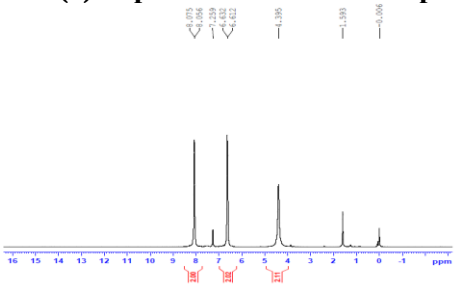

Figure.7. (a) Experimental ^{1}H NMR

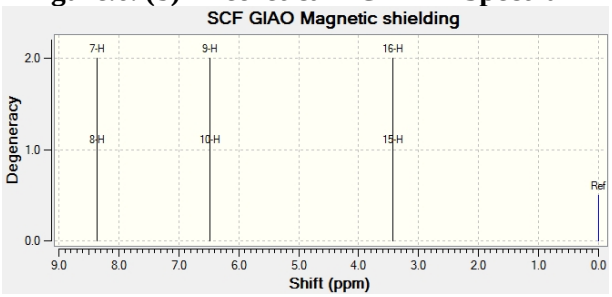

Figure.7. (b) Theoretical ^{1}H NMR Spectrum

Molecular electrostatic potential: In order to study the reactive sites for electrophilic and nucleophilic attack the MEP analysis have been done. In Fig.8, the negative (red and yellow) and the positive (blue) regions of the MEP are consigned to electrophilic reactivity and nucleophilic reactivity respectively. From the Fig.8, it is seen that the negative region is mainly localized over the oxygen atoms (O13 and O14) of the nitro group. The positive region occurs due to the charge localization on the hydrogen atom of the amine group indicating a possible site for nucleophilic attack (Murray and Sen, 1996). Thus it is predicted that the oxygen atom in the nitro group may act as a reactive site for electrophilic attack and the hydrogen atom in the amine group may act as a reactive site for nucleophilic attack. The electrostatic surface potential of 4NA is displayed in Fig.8a.

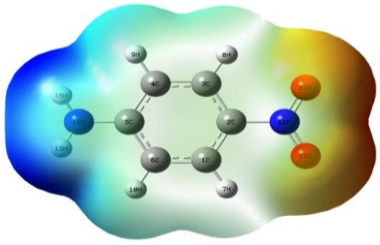

Figure.8. Molecular Electrostatic Potential of 4- NA

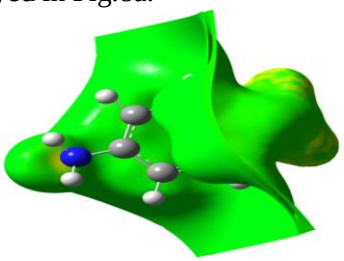

Figure.8a. The electrostatic surface potential of 4-NA

NLO analysis: First order hyper polarizability value was obtained and which has 27 components of the 3D matrix and it is reduced to 10 components with Kleinman symmetry (Andraud, 1994). Calculated hyper polarizability values of 4NA are depicted in Table.4. The calculated first-order hyper polarizability (β_{tot}) value of 4NA is 11.1064 x 10^{-30} esu, which is nearly 56 times greater than the urea (0.1947x10^{-30} esu). This reveals that 4NA compound may be a good candidate for frequency doubling process also it clearly indicates the direction of charge delocalization.

Table.4. Non-linear optical parameters of 4NA calculated using B3LYP/6-31+G (d, p)

Parameters	B3LYP/6-31+ G (d, p)	Parameters	B3LYP/6-31+G (d, p)	Parameters	B3LYP/6-31+G (d, p)
μx	-0.2122886	α_{xx}	45.88447	β_{xxx}	-1.4561619
μy	-2.8023508	α_{xy}	-2.147577	β_{xxy}	-38.3193186
μz	0.1512606	α_{yy}	139.11520	β_{xyy}	-68.5482425
μ_{Total}	2.814447766	α_{xz}	26.591917	β_{yyy}	1466.6682185
		α_{yz}	0.8780031	β_{xxz}	-0.5663166
		α_{zz}	74.0431897	β_{xyz}	-60.3623228
		α_{tot}(esu)	3.3196966X10^{-23}e.s.u	β_{yyz}	26.5562088
				β_{xzz}	0.607684
				β_{yzz}	-103.4717424
				β_{zzz}	4.6123736
				β_{tot} (esu)	11.1064×10^{-30}e.s.u

Powder SHG measurement: Kurtz and Perry (1968), Powder technique was experimentally used to determine the behavior of second harmonic generation of the grown crystal. The sample was beached into fine particles and packed tightly in a micro capillary tube. It was placed in in-front of Nd: YAG laser which has beam energy of 4.7mJ/Pulse and the pulse width of 10ns. It was observed that, the output voltage was 385mV for the 4NA crystal and the value of KDP was 120mV. The relative SHG efficiency of 4-NA crystal is 3 times higher than that of the KDP crystal.

HOMO-LUMO analysis: The Molecular orbital (MO) surfaces have been plotted to realize the bonding scheme of the 4NA compound and it is given in Fig. 9. Details about the molecular stability can also be investigated by analysing the HOMO-LUMO gap. The HOMO-LUMO energy gap value is 0.15866 eV for 4NA molecule. The self-consistent field (SCF) energy of 4NA is -492.122 a.u. The values of electronegativity, hardness (η), softness (ζ) and electrophilicity index (ψ) that are obtained for title molecule are -0.15781, 0.15781, 3.0725 and 7.8589 respectively. Furthermore, low value of HOMO -LUMO energy gap explains the charge transfer interactions that take place within the molecule.

The total density of states (TDOS) spectrum was determined using the Gauss Sum 2.2 program and is visualized in Fig.10. DOS spectrum explains the chemical bonding and molecular orbital compositions. DOS plot confirms that more number of electrons can lodge in the LUMO and the material serves as an electron transport one.

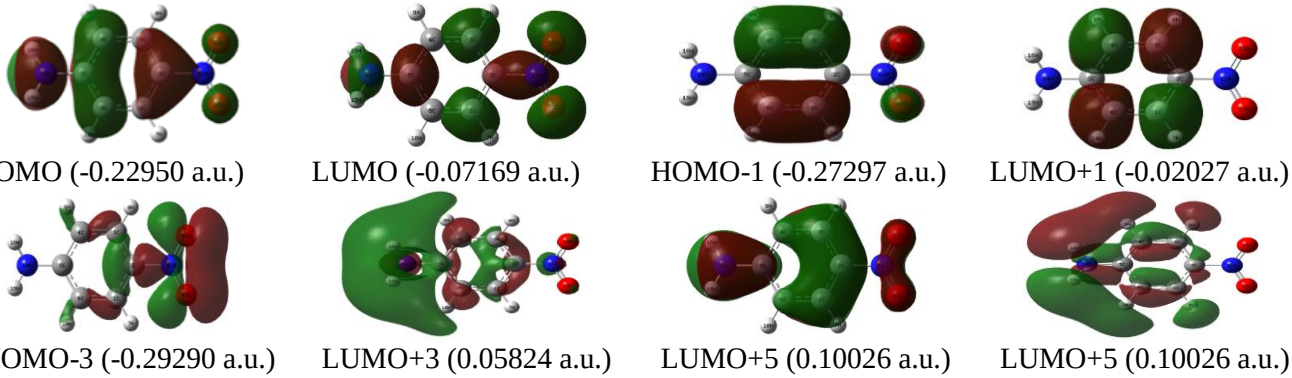

Figure.9. Isodensity plots of the frontier molecular orbitals of 4-NA

Electronic excitation mechanism: The static polarizability value is directly proportional to the optical intensity and inversely proportional to the cube of transition energy (Wu, 2007). Electronic excitation energies and oscillator strength are computed and are given in Table.5. The major contribution from HOMO (-5) to LUMO (+0) is 36% and from HOMO (-3) to LUMO (+0) it is calculated as 27% for the absorption wavelength 257.4 and for energy 4.82eV. Secondly, the major contribution from HOMO (-5) to LUMO (+0) is determined as 27% and from HOMO (-3) to LUMO (+0) it is 20% for the absorption wavelength 219.1 and for energy 5.66eV. Finally, the major contribution from HOMO (-0) to LUMO (+1) is 56% and from HOMO (-1) to LUMO (+0) is 26% for the absorption wavelength 206.2 and energy 6.01eV.

Table.5. Computed absorption wavelength (λ_{ng}), energy (E_{ng}), oscillator strength (f_n) & its contribution

n	λ_{ng}	E_{ng}	f_n	Major contribution
1	257.4	4.82	0.0161	H-5->L+0(+36%), H-3->L+0(27%)
2	219.1	5.66	0.0495	H-5->L+0(+27%), H-3->L+0(20%)
3	206.2	6.01	0.0367	H-0->L+1(+56%), H-1->L+0(26%)

(Assignment; H=HOMO, L=LUMO, L+1=LUMO+1, etc.)

NBO analysis: The second-order Fock matrix has been carried out to evaluate the donor and the acceptor interactions in the NBO basis of 4NA (Krishnakumar, 2014). NBO occupancies at the bond critical points for 4NA compound are gathered in Table.6. The NBO occupancies of C6-C7 bond in 4-NA is larger when compared to other bonds. This reveals that the strength of the bond is high compared to other bonds. Generally in the NBO analysis, the occupancy lies between 0 and 2. In 4NA compound, the bonds C1-C2, C1-C6, C1-H7, C3-C4 and C4-C5 have three occupancy values. The intramolecular interaction occurs due to the orbital overlapping between σ(c-c), σ*(c-c), π(c-c), π*(c-c) bond orbital with intermolecular charge transfer (ICT) which causes the stabilization of the system. These interactions are determined as an increase in Electron Density (ED) in C-C antibonding orbitals and which weakens the respective bonds. Because of these intermolecular charge transfer (σ- σ*, π- π*) large optical nonlinearity is induced in the title molecule.

The important interactions observed in 4NA are lone pair C2 with that of antibonding N11-O13 and the lone pair C5 with that of antibonding, C3-C4 results the stabilization of 621.26 kj/mol and 50.30 kj/mol respectively, which donates larger delocalization. The maximum energy transfer is from LP (C2) and LP (C5) to N11-O13 and C3-C4 as given in Table.6. The bond is conjugated to the anti-bonding orbital of π *(N11-O13) contributing energy of 7.82 kcal/mol.

Table.6. Second order perturbation theory analysis of Fock Matrix in NBO basis corresponding to the intramolecular bonds of 4-NA

Donor(I)	Types of Bond	Occupancy	Acceptor(J)	Type of Bond	Occupancy	E(2) Kcal/Mol	E(i)-E(j) a.u.	F(i,j)
C1-C2	σ	1.97573	C2-C3	σ*	0.02208	4.19	1.27	0.065
			C6-H10	σ*	0.01220	2.44	1.17	0.048
			C1-C6	σ*	0.01306	2.43	1.30	0.050
C1-C6	σ	1.97505	C2-N11	σ*	0.09737	4.32	1.03	0.061
			C1-C2	σ*	0.02208	2.89	1.27	0.054
			C5-C6	σ*	0.02295	2.74	1.25	0.052
C1-H7	σ	1.97771	C2-C3	σ*	0.02208	4.42	1.09	0.062
			C5-C6	σ*	0.02295	4.03	1.07	0.059
			C1-C6	σ*	0.29779	1.19	1.11	0.033
C2-C3	σ	1.97574	C1-C2	σ*	0.02208	4.19	1.27	0.065
			C4-H9	σ*	0.01220	2.44	1.17	0.048
C2-N11	σ	1.99006	C3-C4	σ*	0.01306	1.43	1.39	0.040
			C2-C3	σ*	0.02208	0.75	1.37	0.029
C3-C4	σ	1.97504	C2-N11	σ*	0.09737	4.32	1.03	0.061
			C5-N14	σ*	0.01742	3.51	1.16	0.057
C3-H8	σ	1.97771	C1-C2	σ*	0.02208	4.42	1.09	0.062
			C4-C5	σ*	0.02295	4.03	1.07	0.059
C4-C5	σ	1.97458	C5-C6	σ*	0.02295	3.10	1.24	0.055
			C3-C4	σ*	0.01306	2.51	1.29	0.051
			C3-H8	σ*	0.01371	2.15	1.19	0.045
C4-H9	σ	1.98045	C5-C6	σ*	0.02295	4.04	1.07	0.059
			C2-C3	σ*	0.02208	3.74	1.09	0.057
C5-C6	σ	1.97457	C4-C5	σ*	0.02295	3.10	1.24	0.055
			N14-H16	σ*	0.00772	2.08	1.16	0.044
C5-N14	σ	1.99255	C5-C6	σ*	0.02295	1.49	1.37	0.040
			C1-C6	σ*	0.01306	1.31	1.42	0.038
C6-H10	σ	1.98045	C4-C5	σ*	0.02295	4.03	1.07	0.059
			C1-C2	σ*	0.02208	3.74	1.09	0.057
N11-O12	σ	1.99576	C1-C2	σ*	0.02208	0.93	1.62	0.035
			C2-N11	σ*	0.09737	0.69	1.37	0.028
N11-O13	σ	1.99576	C2-C3	σ*	0.02208	0.93	1.62	0.035
			C2-N11	σ*	0.09737	0.69	1.37	0.028
N11-O13	π	1.98645	N11-O13	π*	0.64836	7.82	0.31	0.054
N14-H15	σ	1.98899	C4-C5	σ*	0.02295	4.12	1.20	0.063
N14-H16	σ	1.98901	C5-C6	σ*	0.02295	4.12	1.20	0.063
LPC2			N11-O13	π*	0.64836	621.26	0.01	0.090
			C3-C4	π*	0.29804	68.86	0.16	0.110
LPC5			C3-C4	π*	0.29804	50.30	0.15	0.098
LPO12			C2-N11	σ*	0.09737	4.47	1.09	0.064
LPO13			C2-N11	σ*	0.09737	4.47	1.09	0.064

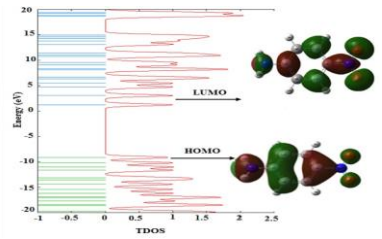

Figure.10. The total density of states of 4NA

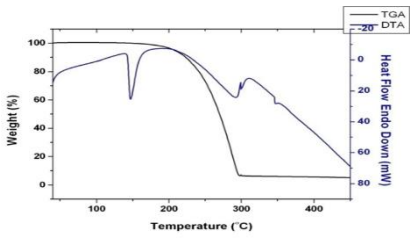

Figure.11. TG/DTA curve of 4-NA

Thermal analysis: Fig.11, shows the TG/DTA curve of 4-NA. It is visible from the TG/DTA graph that the 4NA crystal has thermal stability up to 147°C. From this, it is confirmed that there is no inclusion of solvent in the prepared

material. Only one stage of decomposition was noticed in TGA and in that stage the sample lost almost its 94% of weight. The counter part of this loss was also notice in DTA curve. There is an endothermic peak observed at 147°C which arises due to melting of sample. Apart from that another dip was observed at 345°C which happens due to the boiling of the sample. The sharpness of the endothermic peak observed at 147°C in DTA confirms the quality of 4NA material.

4. CONCLUSION

Optically transparent 4-NA single crystals are grown by slow evaporation method. Monoclinic crystal system of the 4NA crystal was confirmed by XRD analysis. Presence of the functional group and its vibrational nature were analyzed. The 4NA crystal has transparency nature in the range of 390 to 1000 nm and the energy gap value of 4NA is 3.12 eV. The SHG confirms the frequency conversion property and the 4NA crystal has 3 times greater conversion efficiency compare to KDP. The frequency conversion property and transparency nature of 4NA crystal authenticate the appropriateness of the material for optical applications. Molecular analysis authenticate the charge transfer occurs in the molecule when it is excited. Thermal analysis of the material is also studied.

5. ACKNOWLEDGEMENTS

The authors are sincerely thankful to the SHG measurement facility extended by Prof.P.K.Das, IISc, Bangalore. The authors are also thankful to SAIF, IIT, Chennai, Cochin, VIT Vellore and St. Joseph's College, Trichirappalli, India for providing spectral measurements.

REFERENCES

Andraud C, Brotin T, Garcia C, Pelle F, Goldner P, Bigot B, Collet A, Theoretical and experimental investigations of the nonlinear optical properties of vanillin, polyenovanilin and bisvanilin derivatives, J. Am. Chem. Soc, 116, 1994, 2094-2102.

Becke D, Density- functional thermochemistry III, The role of exact exchange, J Chem. Phys, 98 (7), 1993, 5648-5652.

Dillip G.R, Raghavaiah P, Mallikarjuna K, Madhukar C Reddy, Bhagavannarayana G, Ramesh Kumar V, Deva Prasad Raju B, Crystal growth and characterization of γ-glycine grown from potassium fluoride for photonic applications, Spectrochimica Acta part A, 79, 2011, 1123-1127.

Frisch A, Neilson AB and Holder A.J, Gaussview user Manual, Gaussian Inc, Pittsburgh, PA, 2000.

Frisch M.J, Gaussian 09 Revision A.I, Inc, Wallingford CT, 2009.

Hohenberg P and Kohn W, Inhomogeneous Electron Gas, Phy Rev, 136, 1964, B864-872.

Jain M.K, Sharma S.C, Organic Chemistry, Shoban Lal Nagin Chand and Company, Educational Publishers, New Delhi, 1980.

Krishnakumar V, Barathi D, Mathammal R, Balamani J, Jayamani N, Spectroscopic properties, NLO, HOMO–LUMO and NBO of maltol Spectrochim. Acta Part A, 121, 2014, 245–253.

Kurtz S.K, Perry T.T, A Powder Technique for the Evaluation of Nonlinear Optical Materials, J Appl Phys, 39, 1968, 3798-3813.

Lee C, Yang W and Parr R.G, Development of the Colle-Salvetti correlation-energy formula into a functional of the electron density, Phys Rev, B37, 1998, 785-789.

Murray J.S, Sen K, Molecular Electrostatic Potentials, Concepts and Applications, Elsevier, Amsterdam, 1996.

Palafox M.A, Nunez J. L, Gil M, Accurate scaling of the vibrational spectra of aniline and several derivatives, J. Mol. Struct, 593, 2002, 101-131.

Prasad P.N and Williams D.J, Introduction to Nonlinear Optical Effects in Molecules and Polymers, Wiley, New York, 1991.

Rastogi K, Palafox M.A, Tanwar R.P and Mittal L, 3, 5-Difluorobenzonitrile, ab initio calculations, FTIR and Raman spectra Spectrochim Acta A, 58, 2002, 1987-2004.

Rauhut G and Pulay P, Transferable Scaling Factors for Density Functional Derived Vibrational Force Fields, J. Phys. Chem, 99, 1995, 3093-3100.

Williams D.J, Angrew, Organic Polymeric and Non-Polymeric Materials with Large Optical Nonlinearities, Chem. Int. Ed. Engl, 23, 1984, 690-703.

Wu K, Liu C, Mang C, Theoretical studies on vibrational spectra and nonlinear optical property of L-arginine phosphate monohydrate crystal, Opt. Mater, 29, 2007, 1129–1137.